Ultra-narrow ionization resonances in a quantum dot under broadband excitation

S. Gustavsson,[1,2] M. S. Rudner,[3] L. S. Levitov,[4] R. Leturcq,[1,5] M. Studer,[1] T. Ihn,[1] and K. Ensslin[1]

[1] *Solid State Physics Laboratory, ETH Zurich, CH-8093 Zurich, Switzerland*
[2] *Research Laboratory of Electronics, Massachusetts Institute of Technology, Cambridge, MA 02139, USA*
[3] *Department of Physics, Harvard University, 17 Oxford St., Cambridge, MA 02138, USA*
[4] *Department of Physics, Massachusetts Institute of Technology, Cambridge, MA 02139, USA*
[5] *Institute of Electronics, Microelectronics and Nanotechnologies, CNRS-UMR 8520, Department ISEN, 59652 Villeneuve d'Ascq, France*

arXiv:1403.3340v1 [cond-mat.mes-hall] 13 Mar 2014

Semiconductor quantum dots driven by the broadband radiation fields of nearby quantum point contacts provide an exciting new setting for probing dynamics in driven quantum systems at the nanoscale. We report on real-time charge-sensing measurements of the dot occupation, which reveal sharp resonances in the ionization rate as a function of gate voltage and applied magnetic field. Despite the broadband nature of excitation, the resonance widths are much smaller than the scale of thermal broadening. We show that such resonant enhancement of ionization is not accounted for by conventional approaches relying on elastic scattering processes, but can be explained via a mechanism based on a bottleneck process that is relieved near excited state level crossings. The experiment thus reveals a new regime of a strongly driven quantum dynamics in few-electron systems. The theoretical results are in good agreement with observations.

Semiconductor quantum dots with proximal quantum point contacts (QPCs) are versatile systems in which a wealth of quantum dynamical phenomena can be realized and probed [1]. In this work, we employ such a system to investigate ionization in a nanoscale artificial atom (a double quantum dot), using the QPC in a dual capacity as both a broadband emitter[2–4] and as a sensitive time-resolved charge detector [5–10].

Ionization is the process through which a bound electron in a quantum system is ejected to the continuum. Typically, ionization is a *threshold* process, turning on sharply when the quantum of energy in the excitation source exceeds the electronic binding energy. Additional structure in the above-threshold ionization rate may also appear at particular values of the excitation energy due to the presence of quasi-bound excited states (resonances). Such resonances are widely seen in atomic [11, 12], molecular [13], and nanoscale solid state systems [14, 15]. However, when the excitation source has a broad power spectrum, all sharp features of the ionization spectrum are expected to be smeared out.

In contrast to the picture above, in our experiment we find sharp resonances in the ionization rate as a function of gate voltages and external magnetic field. We attribute these features to pairs of excited states that are swept through level crossings when the external fields are varied. Strikingly, even though the radiation is broadband, the observed linewidths are very narrow: converting to an energy scale, we estimate the narrowest lines to be significantly narrower than the thermal broadening $k_{\mathrm{B}}T$ of electron energies in the leads [16, 17].

We stress that the sharp resonances observed in our experiment are of a very different nature from those known e.g. in resonant tunneling in double dots (c.f. Ref. [17]). In our case, resonances appear in a photon-assisted inelastic transport regime, when pairs of *excitation energies* become degenerate; they do not require an absolute alignment of levels in the two dots, and remain sharp even for a broadband distribution of photon energies. Furthermore, the observed resonant enhancement of ionization is not accounted for by models relying on perturbative scattering through the excited states. As discussed in greater detail below, such models predict, quite generally, ionization rates which are independent of level detuning.

To explain the phenomenon, we argue that the resonances arise from a new mechanism, which relies on a bottleneck process that is relieved near the level crossing [Fig. 1a]. The essential ingredients of the model are the existence of a short-lived excited state with strong tunnel coupling to a reservoir, and another state, which is strongly coupled to the ground state by microwave excitation from the QPC. Coupling between these states near a level crossing eliminates a bottleneck for ionization, resulting in a sharp enhancement of the electron escape rate. Crucially, the resonances appear only when the interlevel transitions are strongly driven, near saturation. This is consistent with the observed power-dependence of the experimental traces (see below).

As illustrated in Figs. 1b and 1c, electronic transitions are triggered by non-equilibrium fluctuations emitted from the voltage-biased QPC [18, 19], leading to ionization of the DQD system which we detect in real time by monitoring the conductance of the same QPC [20]. To bring the system into the regime where controlled ionization occurs and where the ionization rate can be measured, we reduce the tunnel couplings between the QDs and source and drain leads to a few kHz. This ensures that the electron dwell times on and off the QDs are longer than the time resolution of the detector ($\tau_{\mathrm{det}} \sim 50\,\mu$s), thus enabling real-time counting of tunnneling events.

In Fig. 2a, we plot the count rate of electrons tunneling into and out of the dot as a function of the potential μ_2 of dot 2 relative to that of the drain lead, measured for several values of V_{QPC}. The peak at $\mu_2 = 0$ is due to equilibrium tunneling back and forth between dot 2

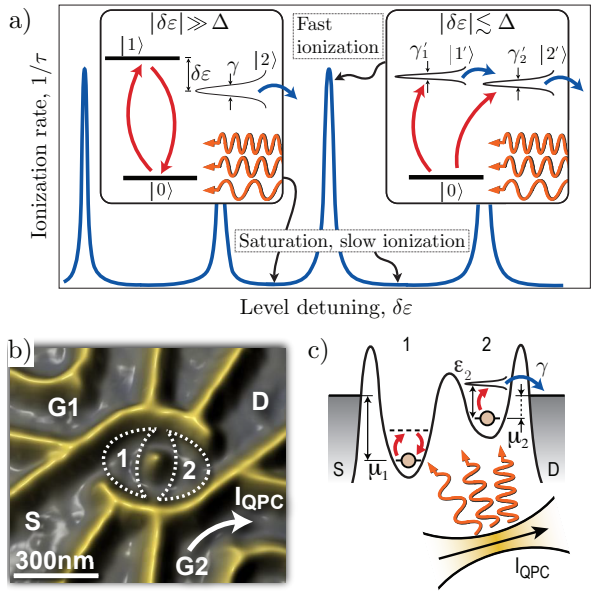

FIG. 1. Resonant enhancement of ionization at a level crossing. a) Broadband radiation from a QPC strongly couples the ground state $|0\rangle$ to an excited state $|1\rangle$. A bottleneck occurs because electron escape to the leads must take place through a different excited state, $|2\rangle$. Near the level crossing, the states $|1\rangle$ and $|2\rangle$ hybridize to form new states $|1'\rangle$ and $|2'\rangle$, Eq.(3). Both states couple to the leads, thus relieving the bottleneck. b) AFM-image of the sample. The structure consists of two quantum dots (marked by 1 and 2) strongly coupled to a sensor/emitter QPC. Each QD contains a few tens of electrons. c) Schematic showing how the model in panel a) arises in a DQD. The many-body excited states $|1\rangle$ and $|2\rangle$ are distributed in both dots, with $|2\rangle$ localized mostly in dot 2 offering the primary coupling to the leads.

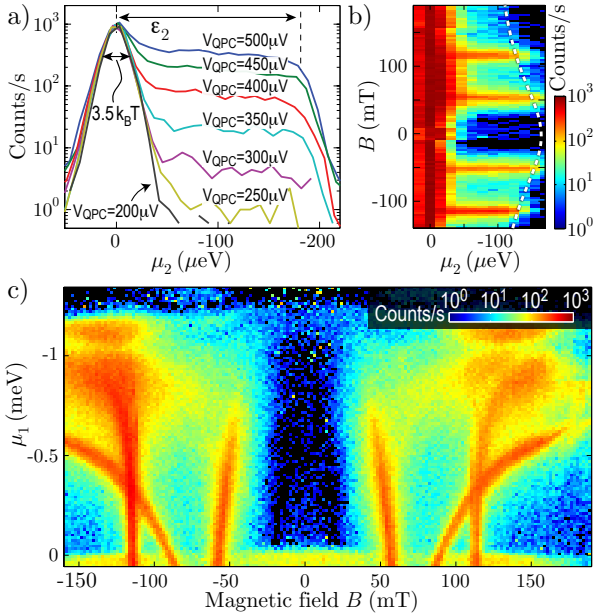

FIG. 2. Ionization measurements of a double quantum dot. a) Number of electrons tunneling in and out of the dot per second, measured as a function of the electrostatic potential of dot 2 (μ_2), relative to the Fermi energy of the drain, for different $V_{\rm QPC}$. The data is taken at $B = 0\,$T, with the potential of dot 1 is fixed at $\mu_1 = -500\,\mu$eV (the values $\mu_{1,2}$ refer to the ground state levels and are obtained from the known capacitive lever arms of the gates [17]). b) Count rate versus μ_2 and magnetic field, measured at $V_{\rm QPC} = 350\ \mu$V and $\mu_1 = -400\,\mu$eV, with dot 1 containing one more electron than in panel a). The region $\mu_2 < 0$ exhibits sharp resonances as a function of magnetic field. c) Ionization rate as a function of magnetic field and dot potential μ_1, with $\mu_2 = -90\ \mu$eV.

and the drain, with the peak height determined by the tunnel coupling and the peak width $3.5\,k_{\rm B}T$ set by the temperature $T = 90\,$mK in the lead[21]. For $|\mu_2| \gg k_{\rm B}T$, equilibrium fluctuations are suppressed. However, fluctuations in the QPC current may also drive inelastic transitions in the DQD when the energy $eV_{\rm QPC}$ supplied by the QPC voltage bias exceeds the required excitation energy [3, 20], giving rise to the broad ionization shoulder seen in Fig. 2a for large values of $V_{\rm QPC}$.

Note that the height of the shoulder is the only feature in Fig. 2a that depends on $V_{\rm QPC}$. Neither the width of the shoulder, corresponding to the excitation energy $\varepsilon_2 = 180\,\mu$eV (see Fig. 1c), nor the shape of the equilibrium peak at $\mu_2 = 0$, are influenced by $V_{\rm QPC}$. Furthermore, the shoulder only appears when $eV_{\rm QPC}$ is larger than ε_2, consistent with the emission spectrum of the QPC[2]. In the appendix we show that only the rate for tunneling out of the QD depends on $V_{\rm QPC}$, thus confirming that the increased count rate originates from ionization by radiation emitted by the QPC.

Using this method for measuring the ionization rate, we now study the rich phenomena that emerge when the excited states of the DQD are tuned by perpendicular (out of plane) magnetic field, B, and gate voltages. Figure 2b shows the electron count rate versus magnetic field and μ_2. Similar to Fig. 2a, the bright vertical feature indicating strong tunneling for $\mu_2 \approx 0$ arises from equilibrium fluctuations between dot 2 and the drain contact, while features at $\mu_2 < 0$ (to the right) indicate inelastic ionization processes. At $B = 0$, the ionization rate is low, displaying only a weak shoulder of enhanced tunneling. At other values of B, however, sharp peaks appear indicating a resonant enhancement of ionization.

It is important to point out that resonances occur when the *excitation energies* in the two dots are equal, $\varepsilon_1 = \varepsilon_2$, irrespective of the absolute alignment of the levels. Thus these features generally would not show up as tunneling resonances in elastic transport through the dots.

The results shown in Fig. 2b are surprising, as both the widths of the resonances (as low as a few mT) and their separations involve magnetic field scales that are much smaller than the fields associated with a flux quantum threading either the ring enclosed by the QDs (120 mT) or one of the QDs (several hundred mT) [22]. Two features in Fig. 2b are particularly illuminating. First, the magnetic field strongly affects the ionization rate within the inelastic shoulder, while having only a weak effect on

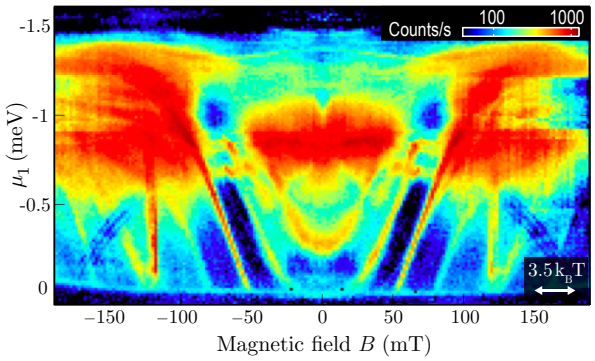

FIG. 3. Ionization resonances as a function of magnetic field and dot potential μ_1, measured for a different charge configuration than in Fig. 2. Many of the resonant features are significantly narrower than the thermal broadening of the electrons in the leads, as indicated by the scale bar in the lower-right corner of the figure. The conversion factor between energy and B-field is 0.8 meV/T.

the shoulder extent (marked by a dashed white line in Fig. 2b). This is consistent with the schematic in Fig.1c, provided that the energy level ε_2 depends only weakly on B. Second, the equilibrium-tunneling peak at $\mu_2 = 0$ displays almost no B-field dependence. Thus, the resonant peaks in ionization cannot be explained by a B-field-induced modulation of the tunnel coupling between a single QD level and the lead.

Further insight into the origin of the resonances can be obtained by tuning the gate voltages, which alters the confining potential of the QDs and changes their excitation spectra. As shown in Fig. 2c, upon sweeping both μ_1 and the magnetic field, different resonances behave essentially independently from each other: some resonances shift strongly with μ_1, while others shift weakly. Interestingly, two of the resonances cross near $B = \pm 115$ mT, displaying no signatures of an avoided crossing (see Appendix). Figure 3 shows the results of a similar measurement, this time obtained with one electron removed from dot 1. Individual resonances shift with B-field and μ_1 in a manner qualitatively similar to that of the resonances in Fig. 2c, but because of a larger number of resonances, the overall picture is more complex. We note that the non-equidistant spacing of the resonances and their B-field dependence make them conceptually different from the phonon-absorption reported in Ref. [23]. The observed response of the resonances to μ_1 and the reshuffling of resonances upon recharging dot 1 suggest that the resonant features arise from excited states in both dots. An example of an energy level configuration leading to such a pattern of resonances is discussed in Appendix E.

How narrow are the resonances? The narrowest peaks in Fig. 3 have full-width half-maxima (FWHM) of about 3 mT, which converted to energy gives an upper bound of 2.4 μeV (see Appendix D). This is substantially lower than the width of the thermally-broadened peak in Fig. 2a, which has a FWHM of $3.5 k_B T = 27\,\mu$eV. To illustrate this comparison, we draw a scale bar in Fig. 3 that corresponds to the FWHM of the thermally-broadened peak.

Below we show that ultra-narrow resonances can be understood within the simple model depicted schematically in Fig.1a. Before proceeding, it is important to point out that a simple perturbative calculation of the ionization rate does not account for the sharp resonances when excited states are nearly degenerate. Formally, this "sum rule" is illustrated as follows. Consider three levels, $|0\rangle$, $|1\rangle$, and $|2\rangle$, corresponding to the DQD ground state and two excited states. The state of the system $|\psi(t)\rangle$ evolves according to $\left[i\frac{d}{dt} - H_0\right]|\psi\rangle = V(t)|\psi\rangle$, with

$$H_0 = \begin{pmatrix} E_0 & \mathbf{0} \\ \mathbf{0} & \mathbf{H_{12}} \end{pmatrix}, \; V(t) = \alpha(t)\Big(|\varphi_{12}\rangle\langle 0| + h.c.\Big). \quad (1)$$

Here $|\varphi_{12}\rangle = C_1|1\rangle + C_2|2\rangle$, with $|C_1|^2 + |C_2|^2 = 1$, and $\mathbf{H_{12}}$ is a 2×2 (non-Hermitian) Hamiltonian accounting for the excited state energies, couplings, and decay rates to the leads (via imaginary level shifts). Broadband radiation is described by $\overline{\alpha(t)\alpha(t')} = W_0\,\delta(t-t')$.

Assuming the system is initialized in the state $|0\rangle$ at time $t = 0$ and setting $E_0 = 0$, we expand $|\psi(t)\rangle$ as $|\psi(t)\rangle = |0\rangle + \int_0^\infty dt' G_0(t-t')V(t')|0\rangle + \cdots$, with $G_0(t-t') = -ie^{-iH_0(t-t')}\,\theta(t-t')$. Keeping terms up to second order in $V(t)$, and averaging over all realizations of the broadband noise, the ionization rate $\Gamma(t) = -\frac{d}{dt}\log\overline{\langle\psi|\psi\rangle}$ is given by $\Gamma(t) = W_0\left[1 - \langle\varphi_{12}|e^{i\mathbf{H_{12}^\dagger}t}e^{-i\mathbf{H_{12}}t}|\varphi_{12}\rangle\right]$ (in the regime $W_0 t \ll 1$ where the perturbative approach is valid). For times longer than the intrinsic excited state lifetimes, the decay rate approaches a constant value $\bar{\Gamma} = W_0$, independent of the details of $\mathbf{H}_{12}$.

Consistency of the approach requires that the excited dot state populations must remain small, implying that the excitation must be weak compared with the smallest escape rate from the excited states. In this case the ionization rate is controlled by coupling of the ground state to the excited states, which, under broadband excitation, is not sensitive to energy level detunings. Thus the ionization resonances are not captured in this approach.

The bottleneck effect responsible for the ionization resonances appears when we consider the *population dynamics* of the 3 level system introduced above. We illustrate the effect with a minimal model in which the broadband noise $V(t)$ primarily couples the ground state and one of the excited states, $|\varphi_{12}\rangle = |1\rangle$ in Eq. (1), while electron escape occurs from the other state, $|2\rangle$. Dynamics within the excited state subspace are described by

$$\mathbf{H_{12}} = \begin{pmatrix} \varepsilon_1 & \Delta/2 \\ \Delta/2 & \varepsilon_2 - i\gamma/2 \end{pmatrix}, \quad (2)$$

where Δ describes the coupling between excited states $|1\rangle$ and $|2\rangle$, with energies ε_1 and ε_2, and γ is the escape rate to continuum. This model describes the generic situation for our system, in which various states typically have very different characteristics. For simplicity, we have set the direct excitation rate to state $|2\rangle$ to zero. More generally,

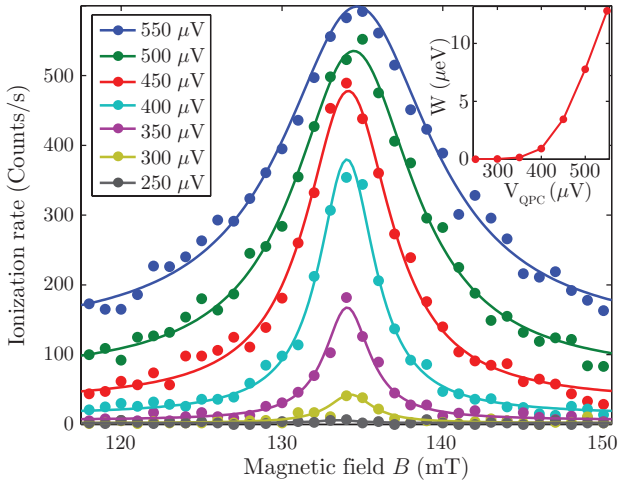

FIG. 4. Line shapes of the ionization resonances. Main panel: ionization rate as a function of magnetic field, measured for different values of $V_{\rm QPC}$. Solid curves are fits to the model, Eqs. (2)-(6), extended to include energy relaxation (see text). The resonance broadens when the excitation rate W exceeds the coupling Δ between the excited states (at $V_{\rm QPC} > 400\,\mu$eV). The fits include a small direct excitation rate (0.5% of W) between $|0\rangle$ and $|2\rangle$, to account for an increase in the background ionization level at high $V_{\rm QPC}$. Inset: excitation rate W, extracted from the fits in the main panel.

resonances appear as long as states $|1\rangle$ and $|2\rangle$ couple differently to the excitation source and to the leads.

We investigate the behavior near level crossing $\delta\varepsilon = \varepsilon_1 - \varepsilon_2 \approx 0$, taking into account the fact that the weak tunnel coupling regime realized in our system, with dwell times on a microsecond scale, is described by $\gamma \ll \Delta$. In this case, suppressing γ and setting $V(t) = 0$, we diagonalize within the excited subspace spanned by $|1\rangle$ and $|2\rangle$ to obtain new hybridized eigenvectors

$$|1'\rangle = \alpha_1|1\rangle + \beta_1|2\rangle, \quad |2'\rangle = \alpha_2|1\rangle + \beta_2|2\rangle. \qquad (3)$$

This yields the eigenvalues $\varepsilon_1' - i\gamma_1'/2$, $\varepsilon_2' - i\gamma_2'/2$, where the decay rates are $\gamma_1' = |\beta_1|^2\gamma$, $\gamma_2' = |\beta_2|^2\gamma$ (see Fig. 1a). The time-dependent field gives rise to nonzero transition rates from the ground state $|0\rangle$ to the excited states $|1'\rangle$ and $|2'\rangle$, given by $w_1' = |\alpha_1|^2 W$ and $w_2' = |\alpha_2|^2 W$, where the net excitation rate W is determined by the power spectrum of $V(t)$.

When the detuning is large, $|\delta\varepsilon| \gtrsim \Delta$, excitation occurs mainly to the non-decaying excited state; the $|0\rangle - |1\rangle$ transition may become saturated, with population transfer from the excited QD state to the continuum acting as a bottleneck for ionization. Near resonance, $|\delta\varepsilon| \lesssim \Delta$, coupling between the excited states relieves the bottleneck and the ionization rate is enhanced. Note that when driving is weak, such that the excitation rate is small compared with $\gamma_{1,2}'$, excitation is the limiting step and no resonant enhancement is expected.

Using the excitation and decay rates defined above, we describe the dynamics of the populations $\mathbf{P} = (P_0, P_1, P_2)^{\rm T}$ of the three states via

$$\dot{\mathbf{P}} = -L\mathbf{P}, \quad L = \begin{pmatrix} w_1' + w_2' & -w_1' & -w_2' \\ -w_1' & w_1' + \gamma_1' & 0 \\ -w_2' & 0 & w_2' + \gamma_2' \end{pmatrix}. \qquad (4)$$

The expected time τ before ionization is given by $\tau = \int_0^\infty (P_0(t) + P_1(t) + P_2(t))dt$. Solving Eq. (F1) as $\mathbf{P}(t) = e^{-Lt}\mathbf{P}(0)$, we have

$$\tau = (111)\left(\int_0^\infty e^{-Lt}dt\right)(100)^{\rm T} = (111)L^{-1}(100)^{\rm T}. \qquad (5)$$

From this expression we find that the net ionization rate $\Gamma(\delta\varepsilon) = \tau^{-1}$ has a Lorentzian dependence on the detuning from level crossing (see Fig. 4):

$$\Gamma(\delta\varepsilon) = \frac{\Gamma_0}{\delta\varepsilon^2 + \gamma_*^2}, \quad \gamma_*^2 = \Delta^2\frac{3W^2 + \gamma^2 + 4W\gamma}{8W\gamma}, \qquad (6)$$

with $\Gamma_0 = \Delta^2(W + \gamma)/8$. Strikingly, the width γ_* of the Lorentzian (6) is a nonmonotonic function of the excitation power W, diverging both in the limit of weak excitation, $W \ll \gamma$, and in the limit of strong excitation, $W \gg \gamma$. The narrowest resonance is realized when the excitation rate W takes an optimal value such that the bottleneck for ionization is due to coupling between unhybridized states $|1\rangle$ and $|2\rangle$. Minimizing γ_*, we find $W = \gamma/\sqrt{3}$. In this case, the width of the resonance equals $\gamma_{*\,\rm min} = \Delta(3^{1/2} + 2)^{1/2}/2 \approx 0.97\Delta$.

In Fig. 4, we plot the measured ionization rates for a resonance similar to the ones shown in Fig. 2 and Fig. 3, for several values of the QPC bias voltage (excitation power). The solid lines indicate fits to a modified form of Eq. (6) which includes the effect of internal relaxation processes from the excited states back to the ground state (see Appendix). Such relaxation, which is not fundamental to the mechanism but appears needed for good quantitative agreement with the experimental observations, limits the efficiency of the ionization process while preserving the Lorentzian form of the resonances. For the fits, we assume the relaxation time $T_1 = 9\,$ns due to phonons [24, 25] to be the same for both excited states, whereas $\gamma = 6\,$peV is known from the time-resolved measurement of the tunneling rate between the excited state in dot 2 and the drain lead. The fitting yields the same coupling $\Delta = 1.3 \pm 0.1\,\mu$eV independent of QPC bias voltage, as expected from the model. The coupling energy is consistent with values typical for resonant tunneling in quantum dot systems [21].

In summary, we have discovered sharp resonances in the ionization rate of a quantum dot driven by broadband radiation. Ionization resonances arise due to a bottleneck process involving pairs of excited states that couple differently to a reservoir and to the microwave excitation, with the state more strongly coupled to the reservoir acting as a probe for other states. General arguments show that such resonances are only expected in a strong driving regime, where the perturbative description based on resonant tunneling between excited states

breaks down. The experiment utilizes the versatility of the coupled QD/QPC system, providing new means for probing strongly driven nanoscale systems.

We thank D. C. Driscoll and A. C. Gossard at Materials Department, University of California, Santa Barbara, California, USA, for fabricating the wafers used in this experiment.

Appendix A: Methods

The device, pictured in Fig. 1b, was fabricated by local oxidation [26] of a GaAs/$Al_{0.3}Ga_{0.7}As$ heterostructure, containing a two-dimensional electron gas located 34 nm below the surface (mobility 3.5×10^5 cm^2/Vs, density 4.6×10^{11} cm^{-2}). The dots are coupled via two separate tunneling barriers, formed in the upper and lower arms between the dots. The charging energy and the energy level spacing are about 1.3 meV and $100 - 200\,\mu$eV for each dot. From the geometry we estimate each QD to contain around 30 electrons. We measured Aharonov-Bohm oscillations in transport to ensure that both barriers are open and have roughly equal tunnel coupling strength [27]. All measurements were performed in a dilution refrigerator with an electron temperature of 90 mK.

In this work, we are tuning the excited state levels ε_1 and ε_2 by applying a perpendicular magnetic field. Since ε_1 and ε_2 are defined relative to the ground state energies μ_1 and μ_2 (see Fig. 1), we first separately determined how μ_1 and μ_2 shift with B-field by measuring the resonant tunneling occurring when the ground states align with the Fermi levels in the leads. For all B-field measurements presented in the paper, compensation voltages were applied to the gates *G1* and *G2*, to always keep the ground states aligned with the leads at $\mu_1,\ \mu_2 = 0$.

Appendix B: Tunneling rates for entering and leaving the QDs

In Fig. 5, we plot the rates $\Gamma_{\rm in}$ and $\Gamma_{\rm out}$ for electrons tunneling into and out of the QD. The rates were extracted from the same set of data as in Fig 2a in the main paper, taking the finite bandwidth of the detector into account [28]. At the position marked by I in Fig. 5, the tunneling is due to equilibrium fluctuations and the rates for tunneling into and out of the QDs are equal. In the regime of QD excitations (case II in Fig. 5), the rate related to absorption ($\Gamma_{\rm out}$) increases strongly with bias voltage over the QPC. Continuing to case III, when $|\mu_2| > \varepsilon_2$ the excited state drops below the Fermi level of the source lead and the absorption rate drops quickly. At the same time, $\Gamma_{\rm in}$ increases as the refilling of an electron into QD2 may occur through either the ground state or the excited state. The rate for tunneling into the $\Gamma_{\rm in}$ does not show any major QPC bias dependence over the full range of the measurement. This is expected, since the refilling of an electron into the QDs does not require absorption of energy.

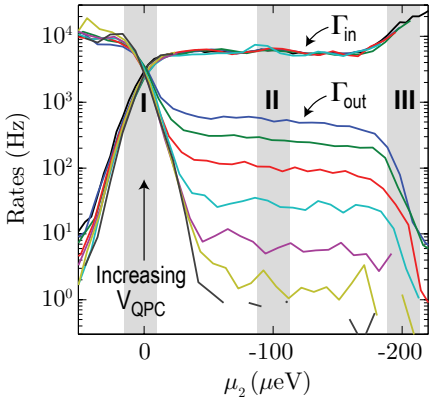

FIG. 5. Rates for electrons tunneling into and out of the QD. The QPC bias is ranging from $V_{\rm QPC} = 200,\ 250,\ 300,\ \ldots,\ 500\,\mu$V.

Appendix C: Magnification around crossing of resonances

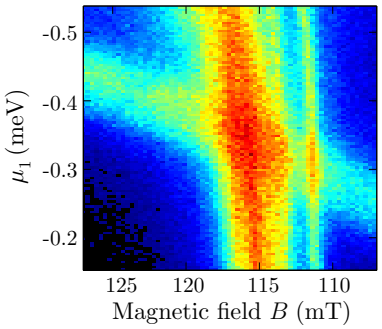

FIG. 6. Magnification of a region in Fig. 2c in the main paper. The vertical line is split into two, with the finer structure having a width below 1 mT. The data is plotted on a linear linear color scale ranging from 0 to 500 counts/s.

Figure 6 shows a magnification of the region around the crossing of resonances in Fig. 2c in the main paper. The vertical feature is found to be split into two peaks, with the smaller sub-peaks having a full-width half maximum below 1 mT. There is no anticrossing visible in the regime where the two main resonances meet. Within the resolution of the measurement, the two resonances appears to be uncoupled.

Appendix D: Estimating the width of the resonances

The narrowest resonances seen in Fig. 3a in the main paper have a full-width half maximum (FWHM) of around 3 mT. To convert this width to an energy scale,

we estimate the energy shift required to bring different states into resonance by changing the B field. The orbital shift of the QD levels with B is given by $\Delta E/B_0 \lesssim 0.4\,\mathrm{meV/\,T}$, where $\Delta E = 100-200\,\mu\mathrm{eV}$ is the level spacing and $B_0 = 500\,\mathrm{mT}$ is the magnetic field associated with a flux quantum threading one of the dots. This is an upper bound for the shift, since hybridization of the orbital states generally leads to flattening of the bands [29], but the value is consistent with the shift marked by the dashed line in Fig. 2b. For two states shifting in opposite directions, we estimate an upper bound of $0.8\,\mathrm{meV/\,T}$ for the conversion factor from magnetic field to energy. This yields an upper bound of $2.4\,\mu$eV for the FWHM of the narrowest features in Fig. 3, thus substantially lower than the width of the thermally-broadened peak in Fig. 2a, which has a FWHM of $3.5k_\mathrm{B}T = 27\,\mu$eV. To illustrate this comparison, we draw a scale bar in Fig. 3 that corresponds to the FWHM of the thermally-broadened peak. Since the states shift differently with magnetic field, the scale bar only serves as a lower bound for the energy resolution due to the thermal broadening. Still, it is clear that several of the resonances in Fig. 3 are considerably narrower than that lower bound.

Appendix E: Model of energy levels giving the positions of the level crossings as a function of magnetic field and gate voltage

In the main text we argue that the resonances correspond to level crossings between excited states in the two dots. Here we describe a plausible configuration of energy levels which yields a similar pattern of resonances to that observed in the data. Unfortunately, the data at hand does not provide enough information to uniquely determine the energy spectrum of the two quantum dots. Instead, the purpose of this section is to show that a simple model involving a few excited states with uncomplicated gate voltage dependence is enough to re-create the fairly complex resonance curves seen in the experimental data.

We start with the experimental configuration and resonance data shown in Fig. 2c. A simple scheme involves level crossings between a single excited state coupled to the lead (denoted $|2\rangle$) and a set of three isolated excited states $|1a\rangle$, $|1b\rangle$, $|1c\rangle$, with energies varying differently with gate voltage and magnetic field. The resonances occur whenever the energy ε_2 of state $|2\rangle$ matches the energy of one of the other excited states.

In general, all excited states shift differently as a function of both the magnetic field and the gate voltages. We assume that the state $|2\rangle$ is localized predominantly in dot 2, and that it is strongly coupled to the drain reservoir. The energy ε_2 of this state depends only very weakly on the potential μ_1 that controls dot 1. This is consistent with the characteristics of our device (see Fig. 1 of the main text). With these restrictions, the conditions for the resonances become

$$\varepsilon_2(B) = \varepsilon_{1\alpha}(\mu_1, B), \tag{E1}$$

where $\alpha = \{a, b, c\}$. In the following, we are going to assume that the energies $\varepsilon_{1\alpha}(\mu_1, B)$ are independent of B-field. This assumption is not physically motivated, but rather servers to show that we can re-create the resonance data seen in the experiment with the simplest possible model. With this simplification, Eq. (E1) becomes

$$\varepsilon_2(B) = \varepsilon_{1\alpha}(\mu_1). \tag{E2}$$

The shape of $\varepsilon_2(B)$ is known experimentally from the measurement in Fig. 2b in the main text (dashed line), which is reproduced in Fig. 7a. By combining the measured dependence of $\varepsilon_2(B)$ with the conditions in Eq. (E2), we can determine how the energies $\varepsilon_{1\alpha}$ must shift with potential μ_1 in order to produce the resonances seen in Fig. 2c in the main text. The extracted values of $\varepsilon_{1\alpha}(\mu_1)$ are plotted in Fig. 7b, and the resulting positions of the crossings $\varepsilon_2 = \varepsilon_{1a}$, ε_{1b}, ε_{1c} as a function of magnetic field and gate voltage are shown in Fig. 7c.

Despite the simplicity of the model, the curves reproduce the pattern of resonances in Fig. 2c of the main text. However, we stress again that the method does not provide any information about the B-field dependence of ε_{1a}, ..., ε_{1c}, and therefore only serves to show that a simple energy dependence is enough to re-create the complex resonance maps seen in the experimental data. A similar approach can be used to re-create the resonance conditions for the data shown in Fig. 3 of the main text.

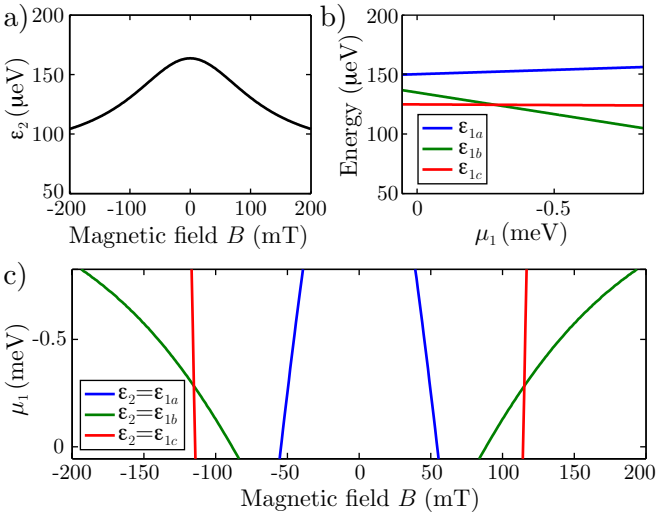

FIG. 7. a) Magnetic field dependence of the energy ε_2 of the state $|2\rangle$ that is strongly coupled to the reservoir. The curve is the same as the dashed line in Fig. 2b. b) Gate voltage dependence of the energies of states $|1a\rangle$, $|1b\rangle$ and $|1c\rangle$, chosen so that panel c) reproduces the measured resonances in Fig. 2c. c) Position of the crossings between the state $|2\rangle$ and three states $|1a\rangle$, $|1b\rangle$, $|1c\rangle$ as a function of magnetic field and gate voltage, calculated using the magnetic field and gate voltage dependences in panels a) and b).

Appendix F: Model of ionization resonances

In this section we present the rate equation model used to describe the resonant enhancement of ionization observed near excited level crossings. In terms of the excitation and escape rates $w'_{1,2}$ and $\gamma'_{1,2}$ defined in the main text (below we suppress the primes for notational simplicity), and additional internal relaxation rates $\Gamma_{1,2}$ that describe relaxation from the excited states $|1\rangle$ and $|2\rangle$ to the ground state, the dynamics of the system is described by rate equations for the populations of the three levels:

$$\dot{\mathbf{P}} = -L\mathbf{P}, \quad L = \begin{pmatrix} w_1+w_2 & -(w_1+\Gamma_1) & -(w_2+\Gamma_2) \\ -w_1 & w_1+\gamma_1+\Gamma_1 & 0 \\ -w_2 & 0 & w_2+\gamma_2+\Gamma_2 \end{pmatrix}, \tag{F1}$$

with $\mathbf{P} = (P_0, P_1, P_2)^{\mathrm{T}}$.

The lifetime of the system, i.e. the expected time before ionization, can be found from $\tau = \int_0^\infty (P_0(t) + P_1(t) + P_2(t))dt$. Solving the rate equations (F1) in terms of a matrix exponential as $\mathbf{P}(t) = e^{-Lt}\mathbf{P}(0)$, we have

$$\tau = (111)\left(\int_0^\infty e^{-Lt}dt\right)(100)^{\mathrm{T}} = (111)L^{-1}(100)^{\mathrm{T}}. \tag{F2}$$

Inverting the matrix L and substituting the result into Eq.(F2), we obtain

$$\tau = \frac{(w_1+\gamma_1+\Gamma_1)(w_2+\gamma_2+\Gamma_2) + w_1(w_2+\gamma_2+\Gamma_2) + w_2(w_1+\gamma_1+\Gamma_1)}{w_1\gamma_1(w_2+\gamma_2+\Gamma_2) + w_2\gamma_2(w_1+\gamma_1+\Gamma_1)} \tag{F3}$$

The dependence of τ on the detuning from level crossing $\delta\varepsilon = \varepsilon_1 - \varepsilon_2$ can be analyzed using the expressions for the rotation matrix (Eq. 2 in the main text), giving

$$\gamma_1/\gamma = \sin^2\theta, \quad \gamma_2/\gamma = \cos^2\theta, \tag{F4}$$

$$w_1/W = \cos^2\theta, \quad w_2/W = \sin^2\theta, \tag{F5}$$

with

$$\cos 2\theta = \delta\varepsilon/\sqrt{\delta\varepsilon^2 + \Delta^2}. \tag{F6}$$

Substituting these expression into the equation for τ, we arrive at

$$\tau = \frac{\left(3\frac{W}{\gamma} + \frac{\gamma}{W} + 4 + 8\frac{\delta\varepsilon^2}{\Delta^2}\right) + \frac{4}{\sin^2 2\theta}\left(2\frac{\Gamma_1}{\gamma}\sin^2\theta + 2\frac{\Gamma_2}{\gamma}\cos^2\theta + \frac{\Gamma_1}{W}\cos^2\theta + \frac{\Gamma_2}{W}\sin^2\theta + \frac{\Gamma_1\Gamma_2}{\gamma W}\right)}{W+\gamma+\Gamma_1+\Gamma_2}, \tag{F7}$$

where $\cos^2\theta = \frac{1}{2}(1+\cos 2\theta)$ and $\sin^2\theta = \frac{1}{2}(1-\cos 2\theta)$, with $\cos 2\theta$ defined in Eq.(F6). The result (F7) generalizes the simplified model discussed in the main text, in which Γ_1 and Γ_2 were assumed to be small compared to γ and W, and therefore ignored.

Expression (F7), where $\Gamma_{1,2}$ are allowed to have arbitrary values and in principle arbitrary energy dependence, is rather complicated. For simplicity, we now take $\Gamma_1 = \Gamma_2$, independent of energy, and find a Lorentzian dependence:

$$\Gamma(\delta\varepsilon) = \frac{\Delta^2(W+\gamma+2\Gamma_1)}{\left[8 + 4\left(2\frac{\Gamma_1}{\gamma} + \frac{\Gamma_1}{W} + \frac{\Gamma_1^2}{\gamma W}\right)\right](\delta\varepsilon^2 + \gamma_*^2)}, \quad \gamma_*^2 = \frac{\Delta^2\left(3\frac{W}{\gamma} + \frac{\gamma}{W} + 4\right) + 8\frac{\Gamma_1}{\gamma} + 4\frac{\Gamma_1}{W} + 4\frac{\Gamma_1^2}{\gamma W}}{8 + 4\left(2\frac{\Gamma_1}{\gamma} + \frac{\Gamma_1}{W} + \frac{\Gamma_1^2}{\gamma W}\right)}. \tag{F8}$$

The width γ_* of the Lorentzian (F8) now has a more complicated dependence on parameters than in the absence of relaxation. Solving for the minimum width, found by setting $d\gamma_*/dW = 0$, requires finding the roots of a cubic polynomial. The analysis shows that the dependence of the width γ_* on the excitation strength W is nonmonotonic, reproducing the behavior discussed in the main text, with the narrowest resonance width attained at some finite value of W. We note that Γ_1 provides a cutoff at small W, so that the width of the resonance no longer diverges for small W.

It is important to note that a simple Fermi's Golden Rule (FGR) calculation of the direct ionization rate of the ground state, which does not account for population build-up in the excited states, fails to explain the observed behavior. After integrating the FGR ionization rate over the broadband spectrum of $V(t)$, we obtain a transition rate which is *independent* of the detuning from resonance. Thus taking into account the bottleneck effect in the rate equations is essential for understanding the enhancement of the ionization rate near resonance.

[1] M. Field, C. G. Smith, M. Pepper, D. A. Ritchie, J. E. F. Frost, G. A. C. Jones, and D. G. Hasko, Phys. Rev. Lett. **70**, 1311 (1993).

[2] R. Aguado and L. P. Kouwenhoven, Phys. Rev. Lett. **84**, 001986 (2000).

[3] E. Onac, F. Balestro, L. H. W. van Beveren, U. Hartmann, Y. V. Nazarov, and L. P. Kouwenhoven, Phys. Rev. Lett. **96**, 176601 (2006).

[4] S. Gustavsson, M. Studer, R. Leturcq, T. Ihn, K. Ensslin, D. C. Driscoll, and A. C. Gossard, Phys. Rev. Lett. **99**, 206804 (2007).

[5] L. M. K. Vandersypen, J. M. Elzerman, R. N. Schouten, L. H. Willems van Beveren, R. Hanson, and L. P. Kouwenhoven, Appl. Phys. Lett. **85**, 4394 (2004).

[6] R. Schleser, E. Ruh, T. Ihn, K. Ensslin, D. C. Driscoll, and A. C. Gossard, Appl. Phys. Lett. **85**, 2005 (2004).

[7] T. Fujisawa, T. Hayashi, Y. Hirayama, H. D. Cheong, and Y. H. Jeong, Appl. Phys. Lett. **84**, 2343 (2004).

[8] J. M. Elzerman, R. Hanson, L. H. Willems van Beveren, B. Witkamp, L. M. K. Vandersypen, and L. P. Kouwenhoven, Nature **430**, 431 (2004).

[9] S. Amasha, K. MacLean, I. P. Radu, D. M. Zumbuhl, M. A. Kastner, M. P. Hanson, and A. C. Gossard, Phys. Rev. Lett. **100**, 046803 (2008).

[10] C. Flindt, C. Fricke, F. Hohls, T. Novotny, K. Netocny, T. Brandes, and R. J. Haug, PNAS **106**, 10116 (2009).

[11] R. P. Madden and K. Codling, Phys. Rev. Lett. **10**, 516 (1963).

[12] M. A. Biondi, A. Herzenberg, and C. E. Kuyatt, Physics Today **32**, 44 (1979).

[13] R. P. Madden and A. G. Parr, Appl. Opt. **21**, 179 (1982).

[14] R. H. Blick, R. J. Haug, D. W. van der Weide, K. von Klitzing, and K. Eberl, Appl. Phys. Lett. **67**, 3924 (1995).

[15] T. H. Oosterkamp, L. P. Kouwenhoven, A. E. A. Koolen, N. C. van der Vaart, and C. J. P. M. Harmans, Phys. Rev. Lett. **78**, 1536 (1997).

[16] A. W. Holleitner, R. H. Blick, A. K. Huttel, K. Eberl, and J. P. Kotthaus, Science **297**, 70 (2002).

[17] W. G. van der Wiel, S. De Franceschi, J. M. Elzerman, T. Fujisawa, S. Tarucha, and L. P. Kouwenhoven, Rev. Mod. Phys. **75**, 1 (2003).

[18] M. H. Devoret, D. Esteve, H. Grabert, G. L. Ingold, H. Pothier, and C. Urbina, Phys. Rev. Lett. **64**, 1824 (1990).

[19] S. M. Girvin, L. I. Glazman, M. Jonson, D. R. Penn, and M. D. Stiles, Phys. Rev. Lett. **64**, 3183 (1990).

[20] S. Gustavsson, I. Shorubalko, R. Leturcq, T. Ihn, K. Ensslin, and S. Schoen, Phys. Rev. B **78**, 035324 (2008).

[21] L. P. Kouwenhoven, C. M. Marcus, P. M. McEuen, S. Tarucha, R. M. Westervelt, and N. S. Wingreen, in *Mesoscopic Electron Transport*, NATO ASI Ser. E 345, edited by L. L. Sohn, L. P. Kouwenhoven, and G. Schön (Kluwer, Dordrecht, 1997) pp. 105–214.

[22] S. M. Cronenwett, S. R. Patel, C. M. Marcus, K. Campman, and A. C. Gossard, Phys. Rev. Lett. **79**, 2312 (1997).

[23] G. Granger, D. Taubert, C. E. Young, L. Gaudreau, A. Kam, S. A. Studenikin, P. Zawadzki, D. Harbusch, D. Schuh, W. Wegscheider, Z. R. Wasilewski, A. A. Clerk, S. Ludwig, and A. S. Sachrajda, Nature Physics **8**, 522 (2012).

[24] T. Fujisawa, D. G. Austing, Y. Tokura, Y. Hirayama, and S. Tarucha, Nature **419**, 278 (2002).

[25] J. R. Petta, A. C. Johnson, C. M. Marcus, M. P. Hanson, and A. C. Gossard, Phys. Rev. Lett. **93**, 186802 (2004).

[26] A. Fuhrer, A. Dorn, S. Lüscher, T. Heinzel, K. Ensslin, W. Wegscheider, and M. Bichler, Superl. and Microstruc. **31**, 19 (2002).

[27] S. Gustavsson, R. Leturcq, M. Studer, T. Ihn, K. Ensslin, D. C. Driscoll, and A. C. Gossard, Nano Letters **8**, 2547 (2008).

[28] O. Naaman and J. Aumentado, Phys. Rev. Lett. **96**, 100201 (2006).

[29] A. Fuhrer, S. Luescher, T. Ihn, T. Heinzel, K. Ensslin, W. Wegscheider, and M. Bichler, Nature **413**, 822 (2001).